Asymmetric Supercapacitive Characteristics of PANI Embedded Holey Graphene Nanoribbons

Sonia Grover, Shubhra Goel,[†] Vikrant Sahu,[†] Gurmeet Singh,* and Raj Kishore Sharma*

Department of Chemistry, University of Delhi, Delhi-110007, India

Ⓢ *Supporting Information*

ABSTRACT: In the present study, graphene oxide nanoribbons (GONR) and reduced graphene oxide nanoribbons (RGONR) supported polyaniline (PANI) nanocomposites are synthesized via an *in situ* chemical polymerization method and investigated for supercapacitor electrodes. Electrochemical studies performed by cyclic voltammetry and galvanostatic charge−discharge (GCD) measurements suggest that both nanocomposites possess enhanced specific capacitance (C_{sp} as 740 F/g for GONR/PANI and 1180 F/g for RGONR/PANI at 5 mV/s). GONR/PANI and RGONR/PANI nanocomposites show good rate capability with high C_{sp} upon increasing the current density from 2 to 20 A/g in GCD measurements, approximately 55% decay in C_{sp} value of the nanocomposites is observed compared to pristine PANI (∼70%). The undertaken study signifies enhanced electrical and electrochemical properties of GONR/RGONR supported PANI nanocomposites due to

a synergistic effect of GONR/RGONR and PANI. Furthermore, asymmetric devices are fabricated using GONR/RGONR as the negative electrode, while GONR/PANI and RGONR/PANI are used as the positive electrode, which exhibit significant enhancement in energy density and device performance.

KEYWORDS: *Polyaniline, Graphene oxide nanoribbons, Reduced graphene oxide nanoribbons, Asymmetric supercapacitors, Nanocomposites, In situ chemical polymerization*
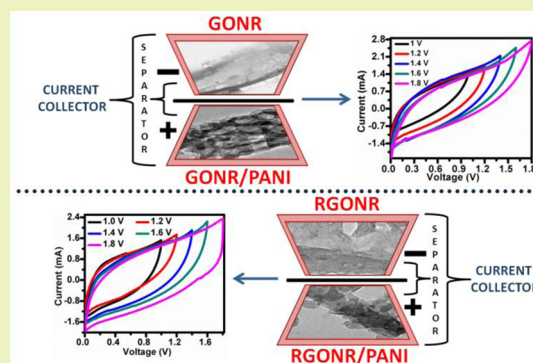
■ INTRODUCTION

While micropower sources are becoming more and more important in our daily life due to the miniaturization of electronics, there has been a considerable interest to develop supercapacitors. Supercapacitors or ultracapacitors store energy as charge and possess excellent cycling stability due to fast charging/discharging rates. On the basis of charge storage mechanisms, supercapacitors can be classified as *electrochemical double layer capacitors* (EDLCs) and *redox capacitors* (or pseudocapacitors). EDLCs exhibit low energy density and high power density, whereas redox capacitors possess high energy density and low power density.[1−3] Various carbon materials, such as carbon black, carbon nanotubes, fullerenes, graphene, etc. are used for EDLCs where charge is accumulated at the electrode−electrolyte interface. While for pseudocapacitors, conducting polymers and metal oxides are used as electrode materials which undergo reversible redox transitions. These transitions go deep inside the bulk and contribute through high pseudocapacitance. Since these transitions involve bulk contribution, the response time for a pseudocapacitor is large compared to that of EDLCs. Besides, it is identified that the combined application of pseudocapacitive and carbonaceous material in supercapacitors significantly improves electrochemical attributes like energy and power density, low response time, etc. In this context, some asymmetric hybrid supercapacitors are being developed in which the positive electrodes

are based on pseudocapacitive materials and different carbon material serving as the negative electrode.[4,5] By assembling two different electrode materials in an electrochemical cell, it is possible to obtain higher working potential which enables the use of a supercapacitor for several applications requiring high potentials.

In the family of conducting polymers, polyaniline (PANI) is a potential candidate for energy storage devices due to its ease of synthesis, environmental stability, fast redox activity, electroactivity, and high specific capacitance (C_{sp}).[6] However, the poor electrochemical stability of PANI as a result of significant volume change due to the shrinkage of polymeric chains during redox cycling limits its applications to a great extent. To overcome such a limitation, various nanocomposites of PANI based on MWCNTs[6,7] and other carbon supports[8] have been developed, which not only enhance the stability of PANI but also maximize its C_{sp} due to the improved network conductivity.

Nowadays, *graphene* has become very popular among the carbon based materials and is extensively used as electrode material for supercapacitors both individually as well as in the form of nanocomposites.[9−12] These "single atom thick" sheets

of hexagonally arranged sp^2 hybridized carbon atoms exhibit exotic in-plane properties like excellent electronic conductivity, high charge mobility, thermal stability, mechanical strength, large specific surface area, and cost-effectiveness as compared to the MWCNTs.[13] Reports are available in the literature about graphene oxide/PANI and reduced graphene oxide/PANI nanocomposites which possess exciting electrochemical properties for energy storage devices.[13−19] For instance, Wang et al. have reported fibrillar PANI doped with graphene oxide sheets having high electrochemical capacitive performance.[13] Gomez et al. have synthesized graphene/PANI nanocomposite electrodes via the chemical precipitation technique for supercapacitor application.[14] Similarly, Yan et al. fabricated graphene nanosheet/PANI nanocomposites using *in situ* polymerization with high C_{sp}.[15] However, most of these works predominantly account for graphene oxide nanosheets derived from graphite flakes, and limited research has been focused on graphene oxide nanoribbons (GONRs) produced via the unzipping of MWCNTs.[20] GONR offer several advantages over graphene oxide nanosheets like the presence of a large number of edges and surface species (functionalities such as COOH, OH, etc.) which make them attractive moieties for covalent functionalization with polymers. The highly active surface area of GONRs enhances the adsorption of a monomer over the nanoribbon surface that consequently enhances the pseudocapacitive contribution to the overall charge storage capacity of nanocomposites. In contrast, reduced graphene oxides (RGOs) are known to exhibit better conductivity and charge storage capacity as compared to graphene oxide due to the removal of functionalities. However, RGOs are required to be dispersed before processing as they get stacked, in order to enhance their performance.

Recently, *lacey* reduced graphene oxide nanoribbons (RGONRs) through chemical opening of MWCNT have been reported by our research group.[21] The work entails the synthesis of novel RGONR with enhanced edge planes consequently enhancing the number of dangling bonds and promoting the dispersion of graphene. In this way, no additional dispersing agent is needed for processing of RGONRs and as such, can be used for charge storage easily. The present research article is focused on synthesis of GONR/ RGONR supported PANI nanocomposites through a similar strategy using an *in situ* chemical polymerization method for supercapacitor electrodes. The energy storage characteristics are investigated via a comparative study of GONR/PANI nanocomposite with those of RGONR/PANI by varying the amount of polymer over the GONR/RGONR. Further, asymmetric devices are fabricated to enhance the energy density using GONR/RGONR as a negative electrode while using GONR/PANI and RGONR/PANI as a positive electrode. Such an assembly significantly enhanced the overall working potential of the supercapacitors.

■ EXPERIMENTAL SECTION

Materials and Methods. *Materials.* MWCNTs (diameter 10−20 nm and length ~1 μm) were purchased from Shenzhen Nanotech Port, Co. Limited, China. All of the chemicals such as aniline, hydrochloric acid (HCl), and ammonium peroxodisulfate (APS) were of GR grade and were used as received.

Synthesis of PANI. PANI was synthesized by a chemical polymerization method reported elsewhere.[18] Aniline dissolved in 20 mL of 1 M HCl solution was kept under vigorous stirring at room temperature. Separately, APS was dissolved in 20 mL of 1 M HCl solution (molar ratio of aniline/APS kept as 1:4) and cooled down to

0−4 °C. Subsequently, the APS solution was added dropwise into the monomer solution and stirred overnight maintaining the temperature at 0−4 °C. Polymerization started within few minutes with the formation of green emeraldine salt in the reaction mixture. The polymerized product was collected by filtration using a cellulose nitrate membrane (0.45 μm) and washed with copious amounts of water. Finally, the sample was dried in a vacuum for 24 h.

Synthesis of GONR/PANI Nanocomposites. GONR was obtained via the unzipping of MWCNTs using an oxidizing mixture (H$_2$SO$_4$/ KMnO$_4$) as earlier reported by Sahu et al.[21] and also depicted in Figure 1. An *in situ* chemical polymerization method was used for the synthesis of GONR/PANI nanocomposites following the same procedure as that adopted for PANI synthesis with the exception that GONR was also added along with an aniline monomer in HCl solution and sonicated for 1 h to make a homogeneous suspension. Thereafter, a precooled solution of APS (molar ratio of aniline/APS kept as 1:4) was slowly added into the above solution and stirred overnight maintaining the temperature at 0−4 °C. The obtained product was filtered using a cellulose nitrate membrane (0.45 μm) and dried in vacuum. The weight ratios of GONR/PANI were varied as 80:20, 50:50, and 30:70 to obtain different compositions of GONR/ PANI nanocomposites. These samples were named as GONR/ PANI20, GONR/PANI50, and GONR/PANI70, respectively.

Synthesis of RGONR/PANI Nanocomposites. The GONR was reduced to give the RGONR through the chemical activation method using KOH at high temperature.[21] Likewise, the GONR/PANI and various RGONR/PANI nanocomposites were synthesized with different weight ratios of aniline using *in situ* chemical polymerization, in the presence of a RGONR suspension as follows. In a set of synthesis, purified aniline was added into a 100 mg suspension of RGONR and sonicated for ~3 h. The solution was stirred in an ice bath maintaining temperature 0−4 °C. Under vigorous stirring, a precooled solution of APS (molar ratio of aniline/APS as 1:4) was added dropwise into the above solution and stirred overnight, maintaining the temperature at 0−4 °C. Afterward, the polymerized product was collected by filtration using a cellulose nitrate membrane (0.45 μm), washed with water, and dried under vacuum. Like the GONR/PANI, different compositions of RGONR/PANI nanocomposites were obtained and named as RGONR/PANI20, RGONR/PANI50, and RGONR/PANI70.

Electrode Preparation. Typically, 5 mg of the sample (GONR, RGONR, PANI, GONR/PANI, and RGONR/PANI) was sonicated with 5 μL of Nafion binder in isopropyl alcohol for 1/2 h and spray coated onto the surface of graphite plates (1 cm × 1 cm). Subsequently, the graphite plates were dried in an oven at 80 °C for 24 h. The weight of the active material loaded over graphite as determined by weighing the graphite plates before and after the spraying/drying process was 0.65 mg/cm^2.

Characterization. High resolution transmission electron microscopy (HRTEM) of the nanocomposites was performed using a Phillips Technai T-300 microscope. Ultraviolet−visible (UV−vis) spectra were recorded in aqueous medium through a UV-160 spectrophotometer. Raman spectroscopy was done by a Renishaw Invia Reflux Micro Raman spectrometer. X-ray diffraction (XRD) data were collected using a D8 DISCOVER high resolution X-ray diffractometer with copper radiation (K_α) of wavelength 1.541 Å, between the 2θ value 10−40° and a scanning speed of 3°/min. Current−voltage (I−V) measurements were carried using pellets (diameter 10 mm) of the material in an indigenous cryostat attached to a Keithley 6517B electrometer in a two-probe setup. Two contacts were made using graphite paste (diameter 1.5 mm), and the distance between these contacts was fixed to 4 mm. All electrochemical measurements were performed at room temperature in a 1 M H$_2$SO$_4$ electrolyte using a three electrode cell with a Pt sheet as the counter electrode and Ag/ AgCl as the reference electrode. The spray-coated electrodes were used as the working electrode. Cyclic voltammetry (CV) and electrochemical impedance spectroscopy (EIS) were carried out using an electrochemical workstation (CHI 604 D). EIS of the electrode materials was performed between the frequency of 10 mHz and 100 kHz at an amplitude of 5 mV. Galvanostatic charge−discharge

(GCD) characteristics were recorded at different current densities using Potentiostat Galvanostat EIS Analyzer PARSTAT 4000. Calculations for specific capacitance (C_{sp}), energy density, and power density were done as described in our earlier article.[22] GONR/PANI50 and RGONR/PANI50 are used for all of the structural as well as electrochemical characterization if the composition is not mentioned.

■ RESULTS AND DISCUSSION

Figure 1 is the schematic representation for the formation of PANI nanocomposites over the GONR/RGONR support. The
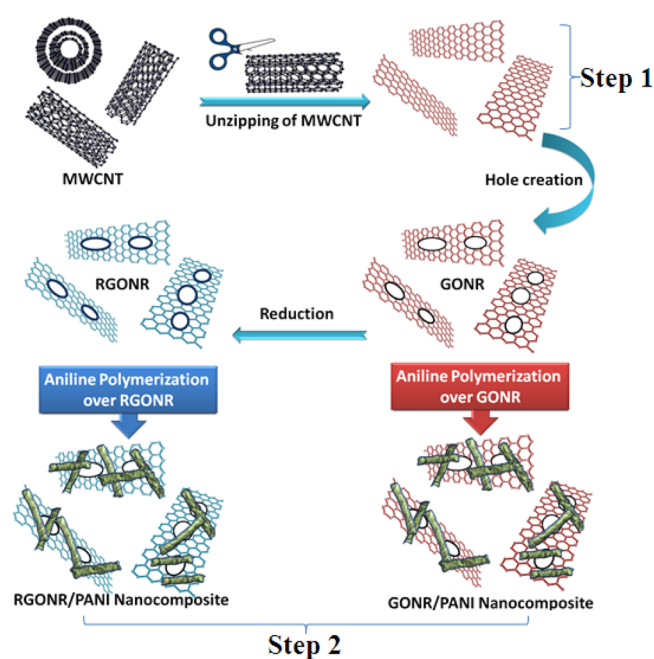

Figure 1. Schematic Representation of the Formation of GONR/PANI and RGONR/PANI Nanocomposites.

nanocomposites were fabricated in two steps as follows. First, the MWCNTs are unzipped using oxidizing mixture H_2SO_4/$KMnO_4$ wherein holes of mesopore diameter sizes are formed in individual ribbons. Our earlier communications clearly describe that the edge planes contain out-of-plane functionalities.[21] These functionalities destack the individual ribbons, however, due to irregular edges these remain in the form of an entangled nanoribbon matrix. In the second step, an *in situ* chemical polymerization of aniline is carried out over both GONRs and RGONRs. The aniline monomer gets adsorbed over the GONR/RGONR surface and then is oxidized via oxidant APS to give GONR/PANI and RGONR/PANI nanocomposites. In the obtained nanocomposites, PANI was deposited all around the nanoribbons of GONR/RGONR to give a highly accessible nanostructured electrode material.

Transmission Electron Microscopy. Figure 2a and b depicts the TEM micrographs of GONR and PANI, respectively, while the micrographs for different wt (%) ratios of GONR/PANI nanocomposites are shown in Figure 2c–e. The TEM micrograph for GONR in Figure 2a shows an intermediate state of *lacey* graphene nanoribbon formation, and it is clearly seen that graphene develops a holey structure and that the individual holey graphene nanoribbons separate from the stack of unzipped MWCNTs. Besides facilitating electrolyte ion migration, the edge planes of these holes carry surface functional groups which anchor the monomer ions and
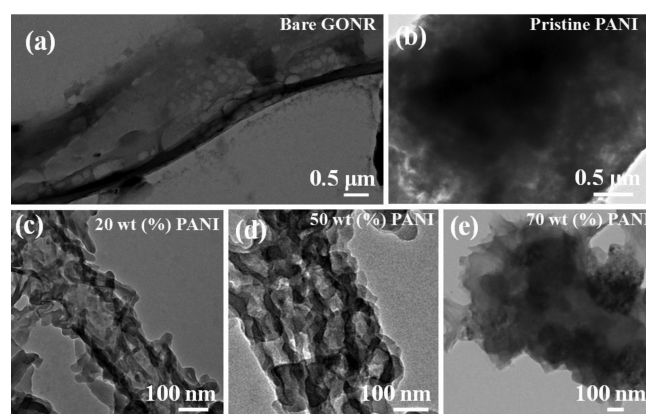

Figure 2. TEM micrographs of (a) GONR, (b) PANI, and (c–e) GONR/PANI nanocomposites with 20, 50, and 70 wt (%) PANI, respectively.

subsequently provide a site for polymerization. Figure 2b represents the TEM micrograph of PANI prepared without the nanoribbon support. The microstructure reveals the bulky and irregular morphology of typical polymeric structures. Interestingly, when the nanoribbons were used as a support during polymer growth, PANI instead of forming a bulky morphology crystallized in the form of ordered nanofibers. The 20 wt (%) PANI nanofibers uniformly covered the GONR surface as evidenced in the TEM micrograph of GONR/PANI in Figure 2c. A remarkable finding of the work is the ordered growth of PANI fibers at the edge planes of an individual nanoribbon. Consequent to the anchoring action of the edge plane functionalities, the nanofibers appear oriented along the axial direction of the nanoribbon. Since the nanoribbons are entangled structures (4–5 layers of stacked graphene with holes) and the intergraphene spacing is accessible to the electrolyte/monomer solution, the growth of PANI fibers inside the entangled structure appears light. However, the fibers placed on the top surface of a nanoribbon appeared dark in contrast as depicted in Figure 2c. This wrapping-up of PANI over GONR is prominent and reaches a maximum extent in the case of the GONR/PANI having PANI as 50 wt (%), as shown in Figure 2d. It is clear from the micrographs that the separated nanoribbons of graphene oxide in Figure 2a have provided an anchoring platform to aniline molecules and act as an effective site/substrate for polymerization and subsequently the crystallization.

Further increase in PANI loading has deleterious effects on the morphological characteristics of GONR/PANI. The TEM micrograph of GONR/PANI with 70 wt (%) PANI loading in Figure 2e shows that the nanocomposite having 70 wt (%) PANI exhibits fully disordered microstructure. The 70 wt (%) loading of PANI completely wrapped the GONR, and it emerged as a highly agglomerated structure with no visibility of the ribbon-like arrangement of GONR/PANI. The results signify the upper limit as 50–60 wt (%) of PANI loading on GONRs as an effective matrix.

In order to investigate the morphological relationship of PANI with the reduced form of graphene nanoribbon (RGONR), Figure 3a–d shows the comparative study with the GONR/PANI nanocomposites. TEM micrographs of RGONR/PANI nanocomposites having similar weight ratios of PANI such as 20%, 50%, and 70% were obtained. Likewise, in the GONR/PANI, the images depict 50–60 wt (%) as
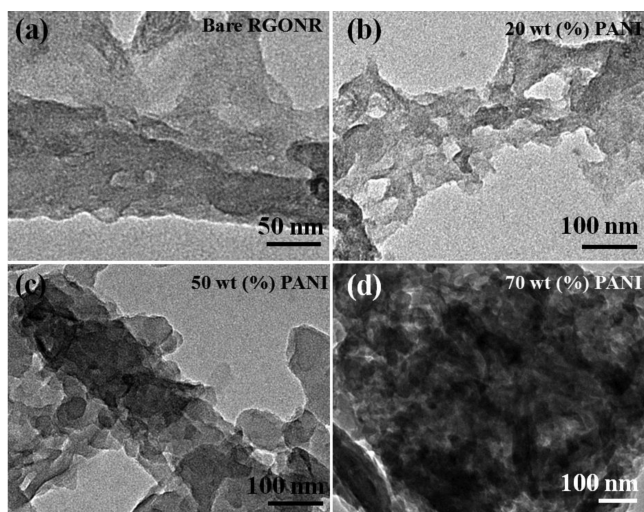
Figure 3. TEM micrographs of (a) RGONR and its nanocomposite with (b) 20 wt (%), (c) 50 wt (%), and (d) 70 wt (%) PANI.

optimal amount for loading PANI to give an interlinked RGONR/PANI matrix. An increase in loading of PANI beyond ~50 wt (%) leads to the formation of an agglomerated structure. To further examine the interaction of GONR/RGONR with PANI, UV−vis and Raman analysis were carried out.

Spectroscopic Studies. *UV−Visible Spectroscopy.* Figure 4a shows the overlaid UV−vis absorption spectra of the
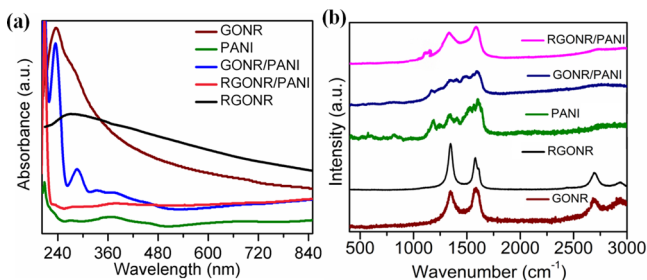

Figure 4. (a) Overlaid UV−visible absorption spectra of GONR, PANI, GONR/PANI, RGONR, and RGONR/PANI. (b) Overlaid Raman spectra of GONR, PANI, GONR/PANI, RGONR, and RGONR/PANI.

GONR, PANI, GONR/PANI, RGONR, and RGONR/PANI in aqueous dispersions. In GONR, the characteristic absorption band at 235 nm is attributed to the $\pi-\pi^*$ transition of aromatic C−C bonds and a weak shoulder at ~275 nm due to the n-π^* transition of C=O bonds of COOH functionalities.[23] For RGONRs, the $\pi-\pi^*$ transition of C−C bonds is observed at a higher wavelength of 272 nm, signifying the reduced state of GONRs.[23] The PANI sample exhibits a sharp and intense absorption band at 208 nm with a weak band at ~270 nm both of which are related to its molecular conjugation.[19,24] Besides, the absorptions at 360 and 450 nm correspond to the electronic transitions from the valence band to the polaron band characteristic of the doped emeraldine state of PANI,[25] which indicates the conducting form of the polymer.

Compared to the optical spectra of GONR and RGONR, the spectra of PANI nanocomposites with GONR/RGONR not only reveal the characteristic bands of PANI but with appreciable change in intensity, reflecting the enhanced

interaction between GONR/RGONR and PANI. For instance, in the case of the GONR/PANI nanocomposite, the absorption bands occur at 232, 333, and 405 nm typical to the GONR and emeraldine state of PANI.[26] Moreover, the band related to the molecular conjugation of PANI exists as sharp intensified peak at a higher wavelength of 285 nm. This red shift can be attributed to the increase in conjugation due to enhanced $\pi-\pi$ interaction between the GONR and PANI.[27,28] Similarly, for the RGONR/PANI nanocomposite, the UV absorption bands appear at 207 and 235 nm typical to PANI and the GONR, respectively. The broad absorption at ~279 nm occurs in RGONR/PANI due to the merging of the characteristic band of reduced GONR and that of conducting PANI.[23] Besides, the absorption observed at a higher wavelength of 370 nm due to $\pi-\pi^*$ transitions of PANI chains reflects strong electrostatic interactions between RGONR and PANI.[28]

Raman Spectroscopy. Figure 4b shows the overlaid Raman spectra of GONR, RGONR, PANI, GONR/PANI, and RGONR/PANI. In the Figure, GONR indicates two prominent peaks at 1348 and 1594 cm^{-1} which correspond to the D and G mode, respectively.[29] The D mode (or phonon mode) arises due to the conversion of the sp^2 hybridized carbon into the sp^3 hybridized carbon (owing to structural defects), while the G mode is related to E$_{2g}$ and is associated with the sp^2 hybridized carbon vibrations.[19,30] For pristine PANI, peaks are observed at 517, 780, 1160, 1217, 1324, 1491, and 1591 cm^{-1} which can be attributed to out-of-plane C−N−C torsion, imine deformation, in-plane C−H bending, in-plane ring deformation, C−N$^{·+}$ stretching, C=N stretching of quinoid, and C−C stretching of benzenoid, respectively.[31,32] The Raman spectrum of the GONR/PANI nanocomposite shows characteristic D and G bands and the peaks corresponding to PANI at 794, 1176, 1255, 1482, and 1591 cm^{-1},[33] indicating the formation of the nanocomposite. However, the spectrum of RGONR/PANI reveals only few characteristic peaks of PANI at ~1160 and 1220 cm^{-1} due to in-plane C−H bending and ring deformation, respectively, while most other bands are suppressed due to the overlapping of RGONR bands with those of PANI. The merging of the peaks occurring at the same position results in such complete overlapping that the characteristic bands for RGONR and PANI are no longer resolvable.

Another noteworthy feature in the spectral details is the I_D/I_G ratio in GONR/PANI and RGONR/PANI nanocomposites that decreases to nearly 0.8 in contrast to that observed for the GONR (0.93) and RGONR (1.4), which signifies that the carbon lattice in the formed nanocomposites contains fewer defects than those of the GONR or RGONR.[29] Because of the removal of functional groups in RGONRs, the graphene ribbons introduce fewer distortions into the carbon lattice. Moreover, because of the interconnected sp^2 carbons, π-electrons delocalize within the ribbons easily and as such, the intensity ratio is higher than the GONR.[21] This further supports the existence of strong $\pi-\pi$ electronic interactions between the GONR/RGONR and PANI due to the formation of ordered structures.[34]

X-ray Diffraction. Figure 5a−d shows the X-ray diffraction patterns of GONR and RGONR, PANI, GONR/PANI, and RGONR/PANI, respectively. Marked differences are observed among the diffraction patterns of these samples. The XRD pattern of the GONR given in Figure 5a signifies an intense and sharp crystalline peak centered at $2\theta = 9.22°$ due to the oxygen containing functional groups present in graphene oxide, with interplanar d-spacing of 0.95 nm. However, for RGONRs the
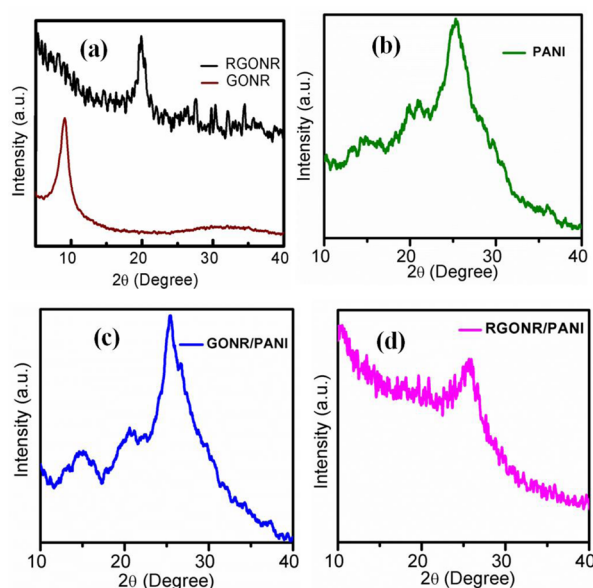
Figure 5. XRD graphs obtained for (a) GONR and RGONR, (b) PANI, (c) GONR/PANI, and (d) RGONR/PANI.

Table 1. Conductivity Values of PANI and Different Ratios of GONR/PANI Nanocomposites along with Their Reduced Counterparts

sample code	ratio of (GONR/RGONR):PANI	conductivity, σ_{RT} (S/m)
GONR	100:0	0.0015
GONR/PANI20	80:20	0.0008
GONR/PANI50	50:50	0.018
GONR/PANI70	30:70	0.030
PANI	0:100	0.008
RGONR	100:0	10
RGONR/PANI20	80:20	0.018
RGONR/PANI50	50:50	0.026
RGONR/PANI70	30:70	0.039

diffraction pattern as depicted in Figure 5a, and the same peak is observed at 25.8° indicating the reduction of GONRs.[18] PANI in Figure 5b shows XRD peaks at $2\theta = 14.46°$ and 19.7° along with a sharp intensified peak situated at 25.6° characteristic to (0 0 1), (0 2 0), and (2 0 0) crystal planes of the emeraldine salt.[35] The XRD graph observed for the GONR/PANI nanocomposite in Figure 5c is somewhat similar to that obtained for pure PANI with the presence of an additional peak of GONR occurring at a lower angle 8.6° and an interplanar distance of 1.04 nm. It can be inferred that the small angle shift of the GONR/PANI nanocomposite is due to the intercalation of PANI on the surface and in-between the graphene oxide nanoribbons. This embedment of PANI into the matrix of GONR possibly increased the interplanar *d*-spacing.[36−39]

A striking feature observed for the RGONR/PANI nano-composite as shown in Figure 5d is the presence of a broad XRD peak at $2\theta = 25°$ due to the merging of crystalline peaks for RGONR along with PANI, which occur at nearly the same positions. The existence of this peak signifies good electrostatic interactions of the RGONR with the PANI molecular chains.

Current-Voltage (I–V) Characteristics. Conductivity measurements were carried out in order to differentiate the interfacial interactions of PANI with GONR/RGONR support. It is observed that the conductivity (σ_{RT}) of GONR/PANI and RGONR/PANI increases with an increase in the wt (%) of PANI. The conductivity values of PANI and GONR/PANI nanocomposites and their reduced counterparts with different ratios are summarized in Table 1.

The conductivity value measured for pristine PANI at the room temperature is nearly 0.008 S/m. However, with increase in PANI loading from 20 to 70 wt (%) in the GONR/PANI nanocomposite, the conductivity increases (from 0.0008 S/m to 0.030 S/m). The remarkable finding of the research is that upon increasing the wt (%) of more resistive PANI, the overall conductivity of the nanocomposite increases. This implies that the PANI which is otherwise resistive by 2/3 order in magnitude compared to that of GONR/RGONR behaves like a good conductor when present over the GONR/RGONR

support. The key reason for resistance in polymeric materials is their arbitrary molecular chain structures. Such structures do not facilitate easy electronic transmission, and often, the electron is shown to follow a complex conduction mechanism like hopping. Electrons require hopping because the polymer chain develops defects like breakings or nonconducting ends.[40−42] Such defects in the polymeric molecular chain inhibit the conducting process, and thus the electron has to find an alternate way to conduct. GONR/RGONR as a conducting support easily accepts the electron and passes it to the current collector; thus, electron hopping is not required, and transmission through the arbitrary molecular chain is bypassed.[43] As shown in Table 1, irrespective of the loading wt (%), conductivity of the GONR/RGONR supported PANI nanocomposites remains dominated by PANI. The fact is attributed to the sandwiched structure of PANI fibers between two GONR or RGONR supports. This structure essentially allows the conduction between two nanoribbons through PANI fibers. Therefore, with the increased PANI loading, conductivity of the nanocomposites increased accordingly. It is understood that with high wt (%), the packing density of PANI fibers between two ribbons increased that consequently increased the number of electrical contacts between the nanoribbons. It is therefore realized that the GONR/RGONR support offers a synergism to the nanocomposite. Hence, there occurs a swift flow of electrons in the nanocomposite through a continued transport pathway assisted by graphene nanoribbons and the synergistic effect of GONR/RGONR for PANI that governs the conductivity of the nanocomposite.

Similarly, upon increasing the PANI wt (%) in RGONR/PANI, the conductive value of nanocomposites is increased from 0.018 S/m to 0.039 S/m. Besides, it is noted that RGONR/PANI nanocomposites exhibit higher conducting behavior than the corresponding GONR/PANI nanocomposites which can be related to the structural defects present in GONR/PANI due to sp^3 hybridization. Conversely, after reduction carbon becomes sp^2 hybridized in the RGONR/PANI nanocomposites. Evidently, the interchain interactions are simply not large enough in GONR/PANI nanocomposites to direct significant delocalization along the matrix.

Electrochemical Studies. *Cyclic Voltammetry.* Cyclic voltammograms and Impedance spectra of pure PANI electrodes were recorded in 1 M H_2SO_4 using three electrode cell assembly (Figures S1 and S2, Supporting Information). Figure 6a shows CV curves of bare GONR and RGONR electrodes in the potential window −0.2 to 0.8 V. It is observed that GONR shows a quasi-reversible curve with a pair of redox
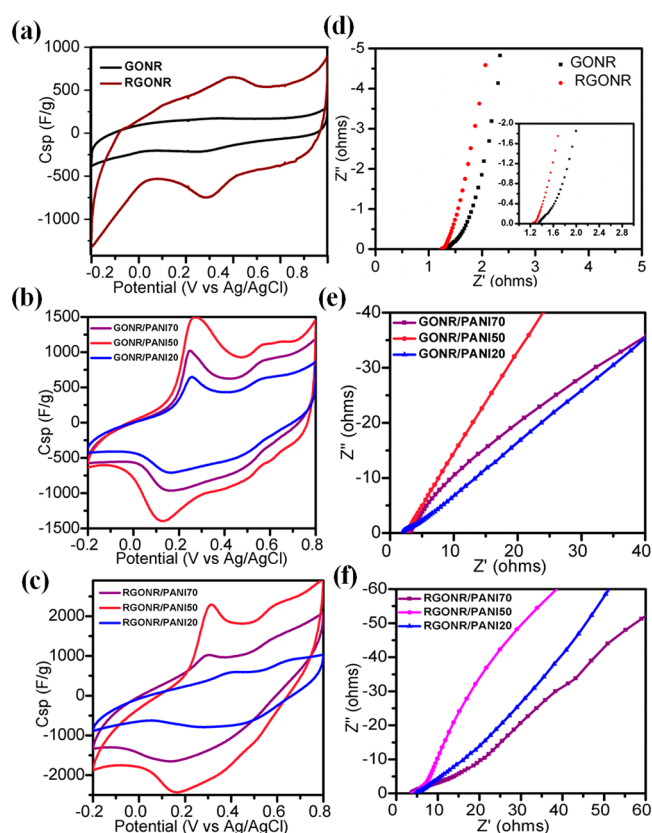
Figure 6. Combined CV's of (a) GONR and RGONR, (b) GONR/PANI nanocomposites, and (c) RGONR/PANI nanocomposites at 5 mV/s. Nyquist plots of (d) GONR and RGONR, (e) GONR/PANI, and (f) RGONR/PANI nanocomposites with different wt (%) of PANI.

RGONR is suggestive of its enhanced charge storage capacity than that of the GONR.

The voltammetric curves of GONR/PANI and RGONR/PANI nanocomposites in different ratios are presented in Figure 6b and c, respectively. For GONR/PANI nanocomposites as shown in Figure 6b, two pairs of redox peaks indicate that their pseudocapacitive behavior is quite different from the EDLC due to the presence of pseudocapacitive PANI in the nanocomposites.[39] Peaks arising below 0.2 V can be ascribed to the redox transition of PANI from a semiconducting state (leucoemeraldine form) to the conducting state (polaronic emeraldine form). However, a pair of peaks observed from 0.4−0.6 V arises due to the faradic transformation of emeraldine (conducting form) to pernigraniline (insulating form).[45] The C_{sp} of the fabricated electrodes GONR/PANI20, GONR/PANI50, and GONR/PANI70 was calculated by integrating the area under the CV curve and deduced as ∼372 F/g, 740 F/g, and 530 F/g, respectively. The increase in C_{sp} of these nanocomposites with increase in PANI up to ∼50 wt (%) is due to the interlinked structure of GONR and PANI, which enhances electrode/electrolyte interface area to facilitate the accessibility of electrolytic ions. Further increase in wt (%) of PANI shows decrement in the charge storage capacity as a result of highly aggregated morphology of the GONR/PANI70 nanocomposite, although its C_{sp} value is higher than that of GONR (220 F/g) and PANI (360 F/g) alone due to synergistic effect.

The area under the CV curves of RGONR/PANI nanocomposites as shown in Figure 6c indicates the C_{sp} of RGONR/PANI20, RGONR/PANI50, and RGONR/PANI70 as ∼427 F/g, 1180 F/g, and 775 F/g, respectively. Herein, the increase in C_{sp} value is observed for RGONR/PANI as compared to the corresponding GONR/PANI nanocomposites due to the combined effect of (1) conducting matrix provided by RGONR, (2) enhanced electrolytic ion accessibility, (3) efficient contribution of EDLC (from RGONR) and pseudocapacitance (from PANI), and (4) less stacked graphene nanoribbons due to the intercalation of PANI during the growth process and reduction of GONR. Table 2 provides a brief literature survey of C_{sp} values exhibited by PANI

peaks corresponding to the −COOH and −OH functionalities.[44] The CV curve of RGONR also shows similar behavior with a pair of redox peaks due to the oxygen containing dangling bonds at the edge defect of the matrix.[21] It may be noted that the enlarged voltammetric area observed for the

Table 2. Comparative Literature Survey of C_{sp} Exhibited by Nanocomposites of PANI with GO/RGO Sheets

S. no.	material used	method used	GO/RGO:PANI	C_{sp} values obtained	ref
1	graphene nanosheets/PANI	microwave solvothermal reduction of GO and chemical polymerization	1:1	408 F/g (5 mV/s)	46
2	graphene/PANI	chemical polymerization	49:1	257 F/g (0.1 A/g)	47
3	PANI nanowires on graphene oxide sheets	chemical polymerization	1:9	555 F/g (0.2 A/g)	48
4	graphene sheets/PANI flakes	chemical polymerization	1:3	GO based nanocomposites: 336 F/g (0.1 A/g); RGO based nanocomposites: 764 F/g (0.1 A/g)	49
5	carboxyl functionalized graphene oxide/PANI nanocomposites	chemical polymerization method	50:1	525 F/g (0.3 A/g)	34
6	electrochemical reduction and oxidation of graphene/PANI nanocomposites	electrochemical polymerization		640 F/g (0.1 A/g)	50
7	graphene/PANI hybrid	chemical polymerization	1:9	1126 F/g (1 mV/s)	51
8	graphene nanosheet/PANI nanofiber composites	chemical polymerization	3:47	1136 F/g (5 mV/s)	52
9	graphene wrapped PANI nanospheres	solution based co-assembly	1:10	615 F/g (1 A/g)	53
10	GONR/PANI and RGONR/PANI nanocomposites	chemical polymerization	1:1	740 F/g and 1180 F/g (5 mV/s)	present study

nanocomposites with GO/RGO sheets synthesized using different techniques. It is examined from the table that the synthesized nanocomposites of the GONR/RGONR with PANI have substantially enhanced electrochemical properties as compared to those of PANI with earlier reported GO/RGO sheets.

Figure 6d shows the combined Nyquist plot of GONR and RGONR. It is observed that both the electrodes show a vertical spike in the high frequency region, indicating pure capacitive behavior. The 45° slope in the Nyquist plot (Warburg resistance) is known to arise from the frequency dependence of ion diffusion/transport in the electrolyte. Herein, the enhanced Warburg region indicates a larger variation in ion-diffusion path length, which consecutively increases the obstruction of ion-movement. Figure 6e and f shows the Nyquist plot of GONR/RGONR nanocomposites with varying ratios of PANI. The curves show that with the increase in wt (%) of PANI, deviation occurs from the ideal capacitive behavior which can be attributed to poor electrical conductivity arising due to the agglomerated structure. However, the low frequency region in the curves of GONR/PANI50 and RGONR/PANI50 nanocomposites is parallel to the y-axis and signifies enhanced capacitive behavior for them as compared to the GONR/RGONR or other ratios of their nanocomposites.

Galvanostatic Charge−Discharge. Figure 7a shows the GCD curves for symmetric supercapacitor devices of PANI,
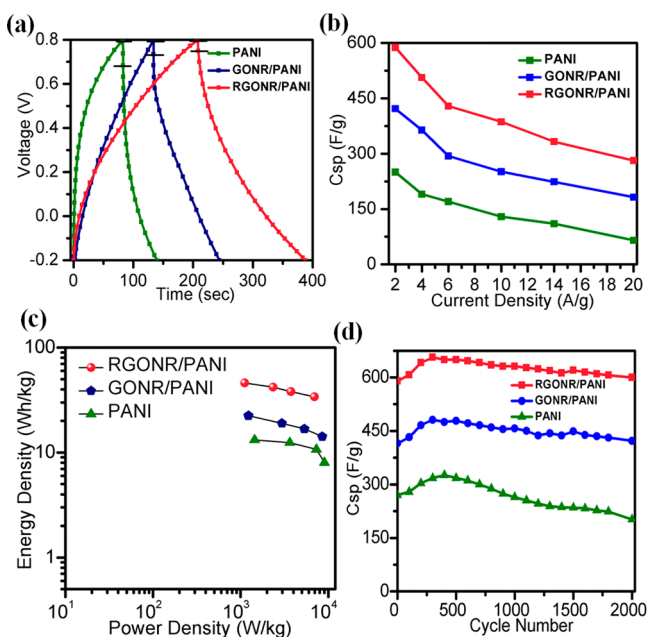

Figure 7. Supercapacitor device characteristics using PANI, GONR/PANI, and RGONR/PANI. (a) GCD curve at 2 A/g, (b) rate capability, (c) Ragone plot, and (d) cycling stability.

GONR/PANI, and RGONR/PANI nanocomposites at 2 A/g in the potential window −0.2 to 0.8 V. The curves indicate symmetrical charging and discharging behavior, which appear to be deviated from linearity due to the pseudocapacitive contribution of PANI. The IR drop is significantly low in RGONR/PANI nanocomposites (0.05 Ω) as compared to pristine PANI (0.12 Ω) and GONR/PANI (0.07 Ω). Furthermore, the total discharge time follows the order as PANI < GONR/PANI < RGONR/PANI, which is in

accordance with their charge storage capacity. The results are consistent with those obtained from CV measurements discussed earlier.

Figure 7b shows the rate capability of GONR/PANI and RGONR/PANI nanocomposites in current density ranging from 2 A/g to 20 A/g. The C_{sp} of the GONR/PANI nanocomposite at 2 A/g is 420 F/g and remains ∼180 F/g even at 20 A/g. However, for the RGONR/PANI nanocomposite it reduces from 590 F/g to 280 F/g at the same current densities. It suggests that both the nanocomposites exhibit better rate capability characteristics than bare PANI, which shows decay in C_{sp} from 250 F/g to 65 F/g. From the data, it is clear that GONR/PANI and RGONR/PANI nanocomposites show 42% and 48% retention in C_{sp}, respectively, compared to 26% of pure PANI. This confirms the synergistic effect of the GONR/RGONR support to PANI in the formed nanocomposites.

The Ragone plot given in Figure 7c reveals significant enhancement in energy density of GONR/PANI (22 Wh/kg) and RGONR/PANI nanocomposites (49 Wh/kg) compared to that of pristine PANI (13 Wh/kg). This increase in energy density can be attributed to the highly interlinked structure of nanocomposites which promotes the electrolytic ion accessibility through the electrode surface. These nanocomposites were further tested for their cycling stability over 2000 cycles at constant current (2 A/g) charge−discharge. Figure 7d shows the cycling life of GONR/PANI and RGONR/PANI nanocomposites and PANI. It is observed that GONR/PANI nanocomposites show 85% retention, while RGONR/PANI nanocomposites exhibited 90% retention in C_{sp} after 2000 cycles. In contrast, the pristine PANI shows only 75% retention in C_{sp}. Thus, both the cycling life and rate capability of PANI are increased by synthesizing its nanocomposites with the GONR/RGONR matrix. The data obtained also supports the conductivity measurements done for the nanocomposites.

It is imperative that the single electrode performance is carried in device functioning as well. Therefore, asymmetric supercapacitor devices of GONR∥GONR/PANI and RGONR∥RGONR/PANI were fabricated with GONR/RGONR as the negative electrode while using GONR/PANI (or RGONR/PANI) as a positive electrode. In the undertaken work, the electrochemical stable potential window of the electrodes was investigated by CV measurements using three electrode cell assembly. Figure 8a shows the CV curves of GONR and GONR/PANI measured in the potential window of −1.0 to 0.0 V and −0.2 to 0.8 V, respectively, at a scan rate 50 mV/s. The voltammogram recorded for GONR is almost rectangular, while the GONR/PANI nanocomposite depicts a slight deviation from the rectangular curve due to the presence of faradic charge contribution from the pseudocapacitive component (PANI). Voltammetry further indicated the stable working potential window for GONR and GONR/PANI nanocomposites as −1.0 to 0.0 V and −0.2 to 0.8 V, respectively. This implies that the lower limit of voltage for GONR is −1.0 V, while the upper limit of voltage for nanocomposites is 0.8 V, which demonstrate that the device fabricated from these two components can accomplish a voltage from −1.0 to 0.8 V without any polarization resistance. Apparently, the maximum working potential limit of a GONR∥GONR/PANI device can be tested up to 1.8 V to achieve better electrochemical performance. Similarly, the maximum potential limit for a RGONR∥RGONR/PANI
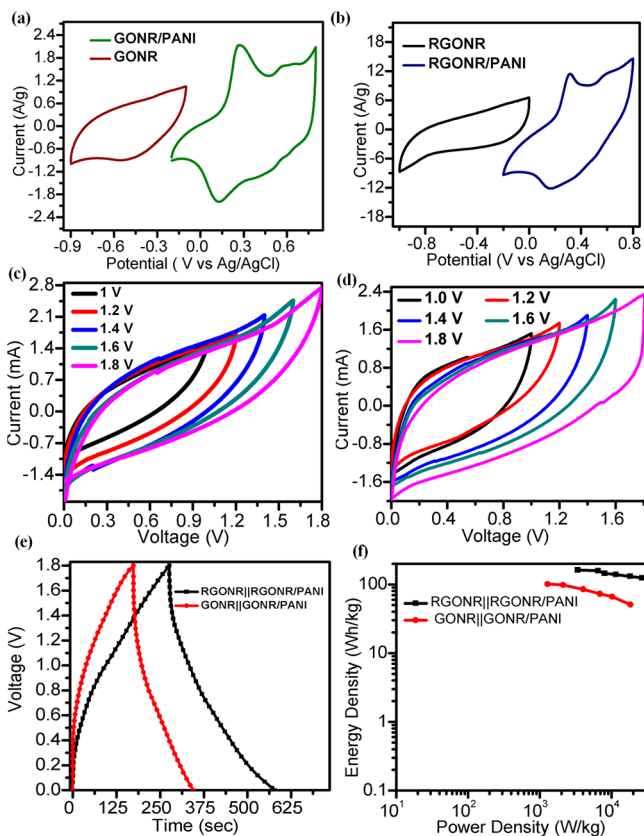
Figure 8. CV curves of (a) GONR and GONR/PANI, and (b) RGONR and RGONR/PANI at 50 mV/s, (c) GONR‖GONR/PANI and (d) RGONR‖RGONR/PANI devices at 10 mV/s, (e) combined GCD curve of an asymmetric device at 2 A/g, and (f) a Ragone plot.

Table 3. Relaxation Time Constant and ESR Values Obtained for PANI, GONR/PANI, RGONR/PANI, and Their Asymmetric Supercapacitor Devices

S. no.	sample	relaxation time (s)	ESR (Ω)	energy density (Wh/kg)	power density (W/kg)
1	PANI	0.068	4.8	13.217	1468.8
2	GONR/PANI	0.056	2.38	23.29	1254.8
3	RGONR/PANI	0.011	3.96	45.55	1107.4
4	GONR‖GONR/PANI	0.009	4.8	99.87	1259
5	RGONR‖RGONR/PANI	0.001	2.66	166	3292

provides information related to the porous structure inside the electrode. It is observed from eq 1 that the τ value of a GONR/PANI (0.056 s) supercapacitor cell is lower than that for bare GONR (0.26 s) and PANI (0.068 s) cells. It can be attributed to the synergistic effect of ordered PANI fiber structure over the GONR, responsible for the improved electrical conductivity of the nanocomposite. In case of the RGONR/PANI nanocomposite, τ is even lower (0.011 s) as compared to the RGONR (0.021 s) and PANI (0.068 s). Results suggest that the application of a relatively better conducting negative electrode helped in lowering ESR that consequently resulted in significantly low relaxation time constant and extended potential range leading to improvement in overall performance of the supercapacitor devices.

CONCLUSIONS

In summary, GONR/RGONR supported polyaniline (PANI)/nanofibers have been synthesized using an *in situ* chemical polymerization method and investigated by different techniques, namely, TEM, UV−vis and Raman spectroscopy, XRD, CV, EIS, and GCD. TEM analysis indicates that 50−60 wt (%) is the optimal amount for loading PANI on GONR/RGONR to give an interlinked structure. Spectroscopic details suggest good $\pi-\pi$ interactions of GONR/RGONR with PANI, which is further supported by the XRD data revealing an increase in interlayer *d*-spacing between layers of GONR and RGONR after the intercalation of PANI. I−V measurements show that both GONR/PANI (0.018 S/m) and RGONR/PANI (0.026 S/m) nanocomposites exhibit higher conductive values as compared to that of PANI alone (0.008 S/m). Electrochemical studies indicate improved performance of GONR/PANI and RGONR/PANI nanocomposites with better charge storage capacity (450 F/g, 770 F/g, and 1180 F/g for PANI, GONR/PANI, and RGONR/PANI, respectively at 5 mV/s), rate capability, and cycling stability compared to those of GONR/RGONR and PANI alone as a result of the synergistic effect of GONR and PANI. Besides, the RGONR/PANI nanocomposites possess significantly enhanced C_{sp} as compared to the corresponding GONR/PANI nanocomposites due to decreased structural defects as a result of sp^2 hybridized carbons in RGONR, which leads to increased C_{sp} values via its marked EDLC contribution. Furthermore, the relaxation time observed for the RGONR/PANI nanocomposite is much lower (0.011 s) than that of RGONR (0.021 s) and PANI (0.068 s) alone. The desired advantages of both molecular systems have been explored by fabricating asymmetric devices, GONR‖GONR/PANI and RGONR‖RGONR/PANI, which have shown significantly enhanced energy density as compared to that of the corresponding symmetric supercapacitor devices. The findings suggest that both GONR/PANI and RGONR/PANI

supercapacitor device can be tested up to 1.8 V as shown in Figure 8b.

Figure 8c and d shows the CVs of asymmetric devices GONR/PANI and RGONR/PANI nanocomposites in different potential ranges up to 1.8 V at a scan rate of 10 mV/s. It is clear from the curves that both of the devices show characteristic electrochemical behavior up to 1.8 V. Figure 8e and f shows the corresponding GCD curves of these devices at a current density of 2 A/g along with the Ragone plots. Significant enhancement in energy density of both the asymmetric devices is observed (99.87 Wh/kg and 163 Wh/kg for GONR/PANI and RGONR/PANI nanocomposites, respectively) in contrast to their corresponding symmetric devices. These investigations suggest that both GONR/PANI and RGONR/PANI nanocomposites can be successfully and efficiently used as electrochemical electrode materials in supercapacitor devices.

The synergistic action of the GONR/RGONR support is clearly seen in Table 3, which displays the electrochemical attributes of the supercapacitor like the relaxation time constant (τ) deduced for symmetric supercapacitor devices and asymmetric supercapacitor devices of the GONR (or RGONR) and GONR/PANI (or RGONR/PANI), equivalent series resistance (ESR), and the energy & power density of the device. The relaxation time constant was calculated by the following equation:

$$\tau = 1/f_0 \tag{1}$$

where, f_0 is the frequency in the bode plot for the supercapacitor device with a phase angle of 45°,[54] and τ

nanocomposites can be used as efficient electrochemical electrode materials for supercapacitors.

ASSOCIATED CONTENT

ⓢ Supporting Information

Electrochemical properties of the PANI electrode were investigated using cyclic voltammetry and impedance spectroscopy in a three electrode cell assembly. The Supporting Information is available free of charge on the ACS Publications website at DOI: 10.1021/acssuschemeng.5b00184.

AUTHOR INFORMATION

Corresponding Authors

*(G.S.) Tel: +91-11-27666616. E-mail: gurmeet123@yahoo. com.

*(R.K.S.) E-mail: drrajksharma@yahoo.co.in.

Author Contributions

†S.G. and V.S. contributed equally to this work.

Notes

The authors declare no competing financial interest.

ACKNOWLEDGMENTS

REFERENCES

(1) Miller, J. R.; Simon, P. Electrochemical Capacitors for Energy Management. *Science* **2008**, *321*, 651−652.

(2) Simon, P.; Gogotsi, Y. Materials for Electrochemical Capacitors. *Nat. Mater.* **2008**, *7*, 845−854.

(3) Chmiola, J.; Yushin, G.; Gogotsi, Y.; Portet, C.; Simon, P.; Taberna, P. L. Anomalous Increase in Carbon Capacitance at Pore Sizes Less Than 1 Nanometer. *Science* **2006**, *313*, 1760−1763.

(4) Fan, Z.; Yan, J.; Wei, T.; Zhi, L.; Ning, G.; Li, T.; Wei, F. Asymmetric Supercapacitors Based on Graphene/MnO2 and Activated Carbon Nanofiber Electrodes with High Power and Energy Density. *Adv. Funct. Mater.* **2011**, *21*, 2366−2375.

(5) Ahuja, P.; Sahu, V.; Ujjain, S. K.; Sharma, R. K.; Singh, G. Performance Evaluation of Asymmetric Supercapacitor Based on Cobalt Manganite Modified Graphene Nanoribbons. *Electrochim. Acta* **2014**, *146*, 429−436.

(6) Frackowiak, E.; Khomenko, V.; Jurewicz, K.; Lota, K.; Beguin, F. Supercapacitors Based on Conducting Polymers/Nanotubes Composites. *J. Power Sources* **2006**, *2*, 413−418.

(7) Yin, Y.; Liu, C.; Fan, S. Well-Constructed CNT Mesh/PANI Nanoporous Electrode and Its Thickness Effect on the Supercapacitor Properties. *J. Phys. Chem. C* **2012**, *116*, 26185−26189.

(8) Bavio, M. A.; Acosta, G. G.; Kessler, T. Polyaniline and Polyaniline-Carbon Black Nanostructures as Electrochemical Capacitor Electrode Materials. *Int. J. Hydrogen Energy* **2014**, *39*, 8582−8589.

(9) Ahuja, P.; Sharma, R. K.; Singh, G. Supercapacitor Using Zinc Manganite Embedded Graphene Nanoribbons. *J. Mater. Chem. A* **2015**, *3*, 4931−4937.

(10) Ujjain, S. K.; Sahu, V.; Sharma, R. K.; Singh, G. High Performance, All Solid State, Flexible Supercapacitor Based on Ionic Liquid Functionalized Graphene. *Electrochim. Acta* **2015**, *15*, 245−251.

(11) Chen, D.; Tang, L.; Li, J. Graphene-Based Materials in Electrochemistry. *Chem. Soc. Rev.* **2010**, *39*, 3157−3180.

(12) Ambrosi, A.; Chua, C. K.; Bonanni, A.; Pumera, M. Electrochemistry of Graphene and Related Materials. *Chem. Rev.* **2014**, *114*, 7150−7188.

(13) Wang, H.; Hao, Q.; Yang, X.; Lu, L.; Wang, X. Graphene Oxide Doped Polyaniline for Supercapacitors. *Electrochem. Commun.* **2009**, *11*, 1158−1161.

(14) Gomez, H.; Ram, M. K.; Alvi, F.; Villalba, P.; Stefanako, E.; Kumar, A. Graphene-Conducting Polymer Nanocomposite as Novel Electrode for Supercapacitors. *J. Power Sources* **2011**, *196*, 4102−4108.

(15) Yan, J.; Wei, T.; Shao, B.; Fan, Z.; Qian, W.; Zhang, M.; Wei, F. Preparation of a Graphene Nanosheet/Polyaniline Composite with High Specific Capacitance. *Carbon* **2010**, *48*, 487−493.

(16) Wang, D. W.; Li, F.; Zhao, J.; Ren, W.; Chen, Z. G.; Tan, J.; Wu, Z. S.; Gentle, I.; Lu, G. Q.; Cheng, H. M. Fabrication of Graphene/ Polyaniline Composite Paper *via in Situ* Anodic Electropolymerization for High- Performance Flexible Electrode. *ACS Nano* **2009**, *3*, 1745− 1752.

(17) Wu, Q.; Xu, Y.; Yao, Z.; Liu, A.; Shi, G. Supercapacitors Based on Flexible Graphene/Polyaniline Nanofiber Composite Films. *ACS Nano* **2010**, *4*, 1963−1970.

(18) Zhang, K.; Zhang, L. L.; Zhao, X. S.; Wu, J. Graphene/ Polyaniline Nanofiber Composites as Supercapacitor Electrodes. *Chem. Mater.* **2010**, *22*, 1392−1401.

(19) Wang, H.; Hao, Q.; Yang, X.; Lu, L.; Wang, X. Effect of Graphene Oxide on the Properties of Its Composite with Polyaniline. *ACS Appl. Mater. Interfaces* **2010**, *2*, 821−828.

(20) Li, L.; Raji, A. R. O.; Fei, H.; Yang, Y.; Samuel, E. L. G.; Tour, J. M. Nanocomposite of Polyaniline Nanorods Grown on Graphene Nanoribbons for Highly Capacitive Pseudocapacitors. *ACS Appl. Mater. Interfaces* **2013**, *5*, 6622−6627.

(21) Sahu, V.; Shekhar, S.; Sharma, R. K.; Singh, G. Ultra High Performance Supercapacitor from Lacey Reduced Graphene Oxide Nanoribbons. *ACS Appl. Mater. Interfaces* **2015**, *7*, 3110−3116.

(22) Grover, S.; Shekhar, S.; Sharma, R. K.; Singh, G. Multiwalled Carbon Nanotube Supported Polypyrrole Manganese Oxide Composite Supercapacitor Electrode: Role of Manganese Oxide Dispersion in Performance Evolution. *Electrochim. Acta* **2014**, *116*, 137−145.

(23) Li, J.; Liu, C. Y.; Liu, Y. Au/Graphene Hydrogel: Synthesis, Characterization and Its Use for Catalytic Reduction of 4-Nitrophenol. *J. Mater. Chem.* **2012**, *22*, 8426−8430.

(24) Xu, L. Q.; Liu, Y. L.; Neoh, K. G.; Kang, E. T.; Fu, G. D. Reduction of Graphene Oxide by Aniline with Its Concomitant Oxidative Polymerization. *Macromol. Rapid Commun.* **2011**, *32*, 684− 688.

(25) Fei, J.; Cui, Y.; Yan, X.; Wang, Y. Y. K.; Li, J. Controlled Fabrication of Polyaniline Spherical and Cubic Shells with Hierarchical Nanostructures. *ACS Nano* **2009**, *3*, 3714−3718.

(26) Mamma, K.; Siraj, K.; Meka, N. Synthesis and Effect of Secondary Dopant on the Conductivity of Conducting Polymer Polyaniline. *J. Polym. Eng.* **2013**, *33*, 785−792.

(27) Rana, U.; Malik, S. Graphene Oxide/Polyaniline Nanostructures: Transformation of 2D Sheet to 1D Nanotube and In-Situ Reduction. *Chem. Commun.* **2012**, *48*, 10862−10864.

(28) Huang, X.; Hu, N.; Gao, R.; Yu, Y.; Wang, Y.; Yang, Z.; Kong, E. S. W.; Wei, H.; Zhang, Y. Reduced Graphene Oxide-Polyaniline Hybrid: Preparation, Characterization and its Applications for Ammonia Gas Sensing. *J. Mater. Chem.* **2012**, *22*, 22488−22495.

(29) Tung, T. T.; Castro, M.; Kim, T. Y.; Suh, K. S.; Feller, J. F. Graphene Quantum Resistive Sensing Skin for the Detection of Alteration Biomarkers. *J. Mater. Chem.* **2012**, *22*, 21754−21766.

(30) Sahu, V.; Grover, S.; Tulachan, B.; Sharma, M.; Srivastava, G.; Roy, M.; Saxena, M.; Sethy, N.; Bhargava, K.; Philip, D.; Kim, H.; Singh, G.; Singh, S. K.; Das, M.; Sharma, R. K. Heavily Nitrogen Doped, Graphene Supercapacitor from Silk Cocoon. *Electrochim. Acta* **2015**, *160*, 244−253.

(31) Markovic, M. G.; Matisons, J. G.; Cervini, R.; Simon, G. P.; Fredericks, P. M. Synthesis of New Polyaniline/Nanotube Composites Using Ultrasonically Initiated Emulsion Polymerization. *Chem. Mater.* **2006**, *18*, 6258−6265.

(32) Wei, Z.; Wan, M.; Lin, T.; Dai, L. Polyaniline Nanotubes Doped with Sulfonated Carbon Nanotubes Made Via a Self-Assembly Process. *Adv. Mater.* **2003**, *15*, 136−139.

(33) Yan, X.; Chen, J.; Yang, J.; Xue, Q.; Miele, P. Fabrication of Free-Standing, Electrochemically Active, and Biocompatible Graphene Oxide-Polyaniline and Graphene-Polyaniline Hybrid Papers. *ACS Appl. Mater. Interfaces* **2010**, *2*, 2521−2529.

(34) Liu, Y.; Deng, R.; Wang, Z.; Liu, H. Carboxyl-Functionalized Graphene Oxide-Polyaniline Composite as a Promising Supercapacitor Material. *J. Mater. Chem.* **2012**, *22*, 13619−13624.

(35) Zhao, Y.; Tang, G. S.; Yu, Z. Z.; Qi, J. S. The Effect of Graphite Oxide on the Thermoelectric Properties of Polyaniline. *Carbon* **2012**, *50*, 3064−3073.

(36) Mahmoud, W. E. Morphology and Physical Properties of Poly(ethylene oxide) Loaded Graphene Nanocomposites Prepared by Two Different Techniques. *Eur. Polym. J.* **2011**, *47*, 1534−1540.

(37) Huang, Y. F.; Lin, C. W. Polyaniline-Intercalated Graphene Oxide Sheet and Its Transition to a Nanotube through a Self-Curling Process. *Polymer* **2012**, *53*, 1079−1085.

(38) Kumar, N. A.; Choi, H. J.; Shin, Y. R.; Chang, D. W.; Dai, L.; Baek, J. B. Polyaniline-Grafted Reduced Graphene Oxide for Efficient Electrochemical Supercapacitors. *ACS Nano* **2012**, *6*, 1715−1723.

(39) Ma, B.; Zhou, X.; Bao, H.; Li, X.; Wang, G. Hierarchical Composites of Sulfonated Graphene-Supported Vertically Aligned Polyaniline Nanorods for High-Performance Supercapacitors. *J. Power Sources* **2012**, *215*, 36−42.

(40) Hu, C. C.; Lin, X. X. Ideally Capacitive Behavior and X-Ray Photoelectron Spectroscopy Characterization of Polypyrrole: Effects of Polymerization Temperatures and Thickness/Coverage. *J. Electrochem. Soc.* **2002**, *149*, A1049−A1057.

(41) Hu, C. C.; Chu, C. H. Electrochemical and Textural Characterization of Iridium-Doped Polyaniline Films for Electrochemical Capacitors. *Mater. Chem. Phys.* **2000**, *65*, 329−338.

(42) Hu, C. C.; Chu, C. H. Electrochemical Impedance Characterization of Polyaniline-Coated Graphite Electrodes for Electrochemical Capacitors-Effects of Film Coverage/Thickness and Anions. *J. Electroanal. Chem.* **2001**, *503*, 105−116.

(43) Sharma, R. K.; Rastogi, A. C.; Desu, S. B. Manganese Oxide Embedded Polypyrrole Nanocomposite for Electrochemical Supercapacitor. *Electrochim. Acta* **2008**, *53*, 5690−5695.

(44) Ban, F. Y.; Majid, S. R.; Huang, N. M.; Lim, H. N. Graphene Oxide and Its Electrochemical Performance. *Int. J. Electrochem. Sci.* **2012**, *7*, 4345−4351.

(45) Obaid, A. Y.; El-Mossalamy, E. H.; Al-Thabaiti, S. A.; El-Hallag, I. S.; Hermas, A. A.; Asiri, A. M. Electrodeposition and Characterization of Polyaniline on Stainless Steel Surface via Cyclic, Convolutive Voltammetry and SEM in Aqueous Acidic Solutions. *Int. J. Electrochem. Sci.* **2014**, *9*, 1003−1015.

(46) Murugan, A. V.; Muraliganth, T.; Manthiram, A. Rapid, Facile Microwave-Solvothermal Synthesis of Graphene Nanosheets and Their Polyaniline Nanocomposites for Energy Storage. *Chem. Mater.* **2009**, *21*, 5004−5006.

(47) Li, Z. F.; Zhang, H.; Liu, Q.; Sun, L.; Stanciu, L.; Xie, J. Fabrication of High-Surface-Area Graphene/Polyaniline Nanocomposites and Their Application in Supercapacitors. *ACS Appl. Mater. Interfaces* **2013**, *5*, 2685−2691.

(48) Xu, J.; Wang, K.; Zu, S.-Z.; Han, B. H.; Wei, Z. Hierarchical Nanocomposites of Polyaniline Nanowire Arrays on Graphene Oxide Sheets with Synergistic Effect for Energy Storage. *ACS Nano* **2010**, *4*, 5019−5026.

(49) Chen, F.; Liu, P.; Zhao, Q. Well-Defined Graphene/Polyaniline Flake Composites for High Performance Supercapacitors. *Electrochim. Acta* **2012**, *76*, 62−68.

(50) Feng, X. M.; Li, R. M.; Ma, Y. W.; Chen, R. F.; Shi, N. E.; Fan, Q. L.; Huang, W. One-Step Electrochemical Synthesis of Graphene/Polyaniline Composite Film and Its Applications. *Adv. Funct. Mater.* **2011**, *21*, 2989−2996.

(51) Wang, H.; Hao, Q.; Yang, X.; Lu, L.; Wang, X. A Nanostructured Graphene/Polyaniline Hybrid Material for Supercapacitors. *Nanoscale* **2010**, *2*, 2164−2170.

(52) Li, J.; Xie, H.; Li, Y.; Liu, J.; Li, Z. Electrochemical Properties of Graphene Nanosheets/Polyaniline Nanofibers Composites as Electrode for Supercapacitors. *J. Power Sources* **2011**, *196*, 10775−10781.

(53) Fan, W.; Zhang, C.; Tjiu, W. W.; Pramoda, K. P.; He, C.; Liu, T. Graphene-Wrapped Polyaniline Hollow Spheres as Novel Hybrid Electrode Materials for Supercapacitor Applications. *ACS Appl. Mater. Interfaces* **2013**, *5*, 3382−3391.

(54) Sellam; Hashmi, S. A. High Rate Performance of Flexible Pseudocapacitors Fabricated using Ionic-Liquid-Based Proton Conducting Polymer Electrolyte with Poly(3,4-ethylenedioxythiophene):Poly(styrene sulfonate) and Its Hydrous Ruthenium Oxide Composite Electrodes. *ACS Appl. Mater. Interfaces* **2013**, *5*, 3875−3883.